



推荐阅读：

[论煤炭绿色开采的地质保障](#)

[我国煤矿区水环境现状及矿井水处理利用研究进展](#)

[西北大型煤炭基地地下水监测背景、思路及方法](#)

[软硬煤复合的煤层气水平井分段压裂技术及应用](#)

[基于排采初期生产特征的煤层气合采地质条件分析](#)

[碎软低渗煤层顶板水平井分段压裂煤层气高效抽采模式](#)

[再论煤矿区生态环境“边采边复”](#)

[西部重点煤矿区土地退化的影响因素及其评估](#)

[采用 HYDRUS 模拟采煤沉陷地裂缝区土壤水盐运移规律](#)

[基于 LBA-BP 的矿井瞬变电磁法岩层富水性的定量预测](#)

[保水采煤面临的科学问题](#)

[西部浅埋煤层开采顶板含水层水量损失动力学过程特征](#)

[神府矿区大型水库旁烧变岩水保水开采技术研究](#)

[生态脆弱区保水采煤矿井\(区\)等级类型](#)

[覆岩破坏充分采动程度定义及判别方法](#)

[干旱矿区采动顶板导水裂隙的演化规律及保水采煤意义](#)

[结构充填“保水-储水”采煤顶板稳定性分析](#)

[基于保水采煤理念的地质环境承载力研究](#)

[西部典型矿区弱胶结地层岩石的物理力学性能特征](#)

[结构充填开采基础理论与地下空间利用构想](#)

[矿井多波多分量地震方法与试验](#)

[煤中稀土元素分布特征及其开发利用前景](#)

[解决矿山环境问题的“九节鞭”](#)

[软硬煤复合的煤层气水平井分段压裂技术及应用](#)

[保水采煤面临的科学问题](#)



推荐阅读：

[西部浅埋煤层开采顶板含水层水量损失动力学过程特征](#)

[神府矿区大型水库旁烧变岩水保水开采技术研究](#)

[生态脆弱区保水采煤矿井\(区\)等级类型](#)

[覆岩破坏充分采动程度定义及判别方法](#)



岳建华,杨海燕,苏本玉,等.矿井张量电阻率法理论基础研究[J].煤炭学报,2020,45(7):2464-2471. doi:10.13225/j.cnki.jccs.DZ20.0938

YUE Jianhua, YANG Haiyan, SU Benyu, et al. Theoretical foundation of tensor measurement for mine resistivity method [J]. Journal of China Coal Society, 2020, 45(7): 2464-2471. doi:10.13225/j.cnki.jccs.DZ20.0938

移动阅读

矿井张量电阻率法理论基础研究

岳建华^{1,2}, 杨海燕¹, 苏本玉¹, 李锋平¹, 刘志新¹, 姜志海¹, 宋雷^{1,2}

(1. 中国矿业大学 资源与地球科学学院, 江苏 徐州 221116; 2. 中国矿业大学 深部岩土力学与地下工程国家重点实验室, 江苏 徐州 221116)

摘要:煤矿采掘活动诱发的局部和微观电各向异性特征时空演变规律有望成为煤矿动力灾害预测预报的新机制。张量电阻率测量是掌握和认识电各向异性特征的重要方法途径,煤矿井下具有开展张量电阻率测量的独特优势。在岩石电各向异性物理机制分析的基础上,结合煤矿井下实际,提出了适合煤矿井下条件的张量电阻率测量方法。以层状各向异性介质模型为例,采用模拟计算的方法对地层倾角、走向变化时的视电阻率方向特性进行了分析;建立了巷道底板岩溶发育全空间模型,从宏观电各向异性的角度分析和验证了电阻率测量所具有的方向性。研究结果表明,采动影响使煤岩体具有电各向异性特征,采动裂隙内的水气富集程度也对煤层横向和纵向电阻率产生明显影响;含水量越大,各向异性系数越高。受上覆和下伏地层电阻率影响,各向异性地层的张量电阻率幅值显示出层状地层的综合反映;其电阻率幅值与裂隙带倾角大小有关,不受地层走向影响,但视电阻率的椭圆分布会随地层走向而发生旋转,旋转的角度依赖于地层走向的变化。这说明采动岩体变形、破坏与流体运移必然会引起含煤地层电各向异性特征的规律性时空演变。通过实时动态测量煤岩体的张量电阻率,可以识别和发现因采掘活动、流体运移引起的局部、微观电各向异性特征。在应力峰值未到达之前,及时捕捉煤矿动力灾害孕育、发展的先兆信息,并在应力释放前的可逆阶段采取预防措施,可从源头上避免煤矿重大动力灾害的发生。

关键词:矿井电阻率法;张量测量;各向异性;煤矿动力灾害

中图分类号:P631 **文献标志码:**A **文章编号:**0253-9993(2020)07-2464-08

Theoretical foundation of tensor measurement for mine resistivity method

YUE Jianhua^{1,2}, YANG Haiyan¹, SU Benyu¹, LI Fengping¹, LIU Zhixin¹, JIANG Zhihai¹, SONG Lei^{1,2}

(1. School of Resources and Geosciences, China University of Mining and Technology, Xuzhou 221116, China; 2. State Key Laboratory for Geomechanics and Deep Underground Engineering, China University of Mining and Technology, Xuzhou 221116, China)

Abstract: The law of temporal and spatial evolution of local or microscopic anisotropy, caused by coal mining, is a key study on coal mine dynamic disaster prediction and prevention. As an important approach to understand the anisotropic characteristics of coal and rock mass, the tensor resistivity measurement has unique advantage in underground mine roadway. Based on the analysis of physical mechanism for rock resistivity anisotropy along with underground roadway circumstances, a mine tensor resistivity method was proposed. Taking the examples of anisotropic layered medium models, the apparent resistivity was calculated with different stratigraphic dips and strikes, and the directional characteristics of which were analyzed. Using a full-space model with Karst development, the directionality of mine resistivity method was analyzed and verified from global anisotropic response view. The results show that it has an anisotropic be-

havior in coal and rock mass under the influence of mining, and the water-gas enrichment status in fracture has an effect on the horizontal and vertical resistivities. The anisotropic coefficient increases with water content. Apparent resistivity amplitude in an anisotropic stratum is affected by its overlying and underlying strata, which reflects a comprehensive response of all layers. Besides, the amplitude can be decided by the fracture zone dips instead of the strikes, however, the elliptic resistivity distribution rotates owing to the strikes change. The results also indicate that the regular temporal and spatial evolution of strata anisotropic behavior is influenced by rock mass deformation and failure, as well as fluid migration. By real-time dynamically measuring the tensor resistivity of coal and rock mass, the local or microscopic anisotropic characteristics caused by mining and fluid migration can be recognized. Capturing auspice signal containing dynamic disaster gestation and development in time before the peak stress arrives, and adopting prevention approach in reversible phase before stress releases, the significant dynamic disasters can be avoided from the source.

Key words: mine resistivity method; tensor measurement; anisotropy; dynamic disaster of coal mine

20世纪80年代末至90年代初井下电阻率法的崛起有效遏止了我国煤矿底板重大突水事故频发的势头^[1-13],而2005—2010年间矿井瞬变电磁超前探测方法与装备的快速发展则为大幅减少老窑采空区等重大透水事故发挥了关键作用^[14-19],目前电阻率法和瞬变电磁法成为矿井地球物理勘探的主力方法。

含煤地层的分层特征使其在宏观上具有结构性电各向异性特征^[6],而煤矿采掘活动诱发的应力转移、煤岩体结构演变、瓦斯和水运移等煤矿动力灾害致灾因素则具有强烈的局部和微观各向异性特征。研究结果表明:断层、裂隙和破碎带等地质构造造成地层的局部电阻率显著增大,一旦地下水渗透至裂隙内,地层的局部电阻率将显著降低。裂隙表面微观粗糙度和宏观开度直接对整体导电性产生影响,粗糙度和开度的大小使得地层的导电性变得复杂^[20-24]。典型煤岩试样和原位测试结果表明,瓦斯突出煤体电阻率是非突出煤体的10倍以上^[25-26],天然地震前兆信息中也有类似反映^[27-28]。然而,在过去30多年的矿井地球物理研究中,人们主要利用宏观电各向异性进行定向探测来确定目标体方位,其观测方式以标量观测为主^[29],无法客观全面地反映采动岩体各向异性特征及时空演变规律,既不利于电性异常区域的精准定位,更错失了为煤岩动力灾害“超前预报、超前解危”提供先兆信息的宝贵机遇。

最新研究进展表明^[30-31],煤与瓦斯突出、冲击地压等动力灾害从孕育、发展到发生的过程经历了应力转移、煤岩变形破坏和流体运移等复杂非线性过程,在这一过程中最显著的物性特征是煤岩体电各向异性的规律性时空演变,且裂隙内水和气所表现出的宏观导电性差异为裂隙充水或瓦斯富含状态的辨识提供了物理依据,从而为利用电法超前预报煤矿动力灾害奠定了物性基础。过去十多年,随着对地球电各向异性特征的深入认识,人们越来越意识到各向同性假

设下的电阻率标量观测具有局限性,针对真实的电各向异性介质开展张量测量已经成为一种必然趋势,并在许多领域得到成功应用^[32-39]。为此,笔者将采用数值模拟方法对煤岩体各向异性响应特征开展研究,为矿井电阻率张量观测方法技术体系的建立及相关装备的研发提供理论依据。

1 电各向异性的物理基础

介质的电阻率 ρ 在很大程度上取决于含水饱和度,其对应关系^[27]为

$$\rho = a\rho_0\varphi^{-P} \left(1 - \frac{V_g}{V_\varphi}\right)^{-m} \quad (1)$$

式中, a 为无量纲的系数; ρ_0 为地层水的电阻率; φ 为岩层的孔隙度; P 在1至2之间; V_g 和 V_φ 分别是岩石内空隙气体和空隙的体积; m 为常量,其值一般取为2。

假设空隙内的空间由水和气充满,即 $V_\varphi = V_g + V_w$,其中 V_w 为地层水所占体积。此时,式(1)可改写为

$$\rho = a\rho_0\varphi^{-P} \left(1 - \frac{1}{1 + r_1}\right)^{-m} \quad (2)$$

式中, r_1 为孔隙中水和气的体积比值,即

$$r_1 = V_w/V_g$$

当地层水电阻率为 $1 \Omega \cdot m$ 时,选择 α 为1.56^[40], $P=1.5$,孔隙度 $\varphi=0.2$,由式(2)计算的电阻率随裂隙内水气体积比变化情况如图1所示。由图1可知,随着裂隙内含水量的增加,裂隙整体电阻率不断减小,并逐渐趋于稳定,电阻率值接近 $17 \Omega \cdot m$ 。当水气体积比 >10 后,孔隙度成为决定电阻率大小的主要因素。

若煤层和煤层内含水裂隙的电阻率分别为 ρ_1 和 ρ ,煤层厚度和裂隙宽度分别为 h_1 和 h ,引入参数 r_2 ,该参数为裂隙宽度与煤层厚度比,用于表示煤层中裂

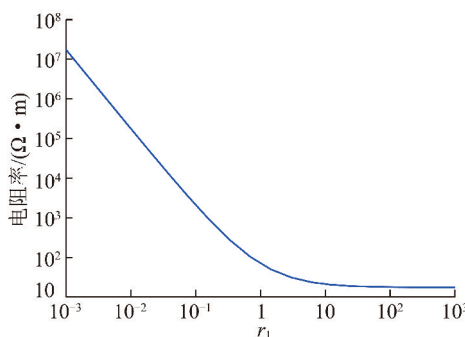


图1 电阻率随裂隙内水气体积比变化曲线

Fig. 1 Resistivity curve with the ratio r_1

隙的相对大小,即

$$r_2 = h/h_1$$

根据克拉耶夫公式^[41],整个煤层的横向电阻率(ρ_n)和纵向电阻率(ρ_t)分别为

$$\rho_n = \frac{2\rho_1 + \rho r_2}{2 + r_2} \quad (3)$$

$$\rho_t = \frac{2 + r_2}{2/\rho_1 + 2r_2/\rho} \quad (4)$$

各向异性系数为

$$\lambda = \sqrt{\rho_n/\rho_t} \quad (5)$$

选择3种水气比率10,1和0.1来代表裂隙内的3种可能状态:以水为主、水气均衡和以气为主,采用式(3)~(5)来计算相应状态下的电阻率和各向异性系数,绘制的图件如图2所示。由图2(a)可以得到:
①虽然横向电阻率只随裂隙宽度变化(即式(3)中裂隙电阻率为固定值),但裂隙宽度因素仍然能对横向电阻率产生较大影响。水气均衡或水含量多时横向电阻率随裂隙宽度增加而缓慢减弱,以气为主时横向电阻率则剧烈上升。
②纵向电阻率受裂隙大小和填充物电阻率控制,水含量大时随裂隙宽度增加急剧减弱,气含量大时随裂隙宽度增加缓慢增大。图2(b)显示出各向异性系数在岩层内产生裂隙时开始逐渐增大,表明此时电阻率开始表现出方向性。对于同样尺度的裂隙,含水量越大,各向异性系数越高。

2 张量电阻率法测量原理

稳恒电流场的电场强度与电流密度间的关系满足欧姆定律,其微分形式为

$$\mathbf{E}_i = \boldsymbol{\rho}^a \mathbf{J}_i \quad (6)$$

$$(E_{3x}K_1 - E_{2x}K_2 + E_{1x}K_3$$

$$E_{3y}K_1 - E_{2y}K_2 + E_{1y}K_3$$

$$E_{3z}K_1 - E_{2z}K_2 + E_{1z}K_3)$$

$$\boldsymbol{\rho}^a = \begin{pmatrix} \rho_{xx}^a & \rho_{xy}^a & \rho_{xz}^a \\ \rho_{yx}^a & \rho_{yy}^a & \rho_{yz}^a \\ \rho_{zx}^a & \rho_{zy}^a & \rho_{zz}^a \end{pmatrix} = \mathbf{E}_i \mathbf{J}_i^{-1} = \frac{(E_{3x}K_1 - E_{2x}K_2 + E_{1x}K_3 \quad E_{2x}K_4 - E_{3x}K_5 + E_{1x}K_6 \quad E_{3x}K_7 - E_{2x}K_8 + E_{1x}K_9)}{(J_{1x}J_{2y}J_{3z} + J_{2x}J_{3y}J_{1z} + J_{3x}J_{1y}J_{2z} - J_{1x}J_{3y}J_{2z} - J_{2x}J_{1y}J_{3z} - J_{3x}J_{2y}J_{1z}) \quad (9)}$$

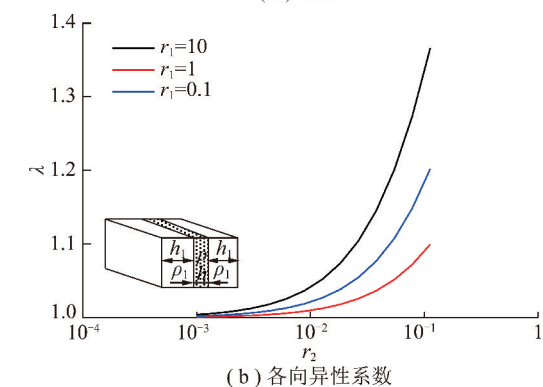
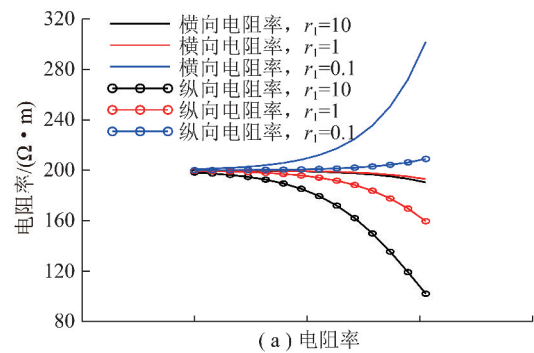


图2 裂隙宽度与煤层厚度比变化时的各向异性曲线

Fig. 2 Anisotropic curves of different slit width and coal seam thickness ratio

式中, \mathbf{E}_i 为电场强度矢量; \mathbf{J}_i 为电流密度矢量; $\boldsymbol{\rho}^a$ 为电阻率张量。

$$\begin{aligned} [E_x] &= [\rho_{xx} \quad \rho_{xy} \quad \rho_{xz}] [J_x] \\ [E_y] &= [\rho_{yx} \quad \rho_{yy} \quad \rho_{yz}] [J_y] \\ [E_z] &= [\rho_{zx} \quad \rho_{zy} \quad \rho_{zz}] [J_z] \end{aligned} \quad (7)$$

为确定电阻率张量的9个分量,可以采用煤矿井下传统电阻率法常用的三极装置,即在巷道顶板、侧帮和底板上分别布置供电电极 A_1, A_2, A_3 ,并采用两两相互垂直的测量电极 M_1, M_2, M_3 ,逐一测量 M_i 与 N 间的电位差。为简化计算,不妨假设供电电极 A_1, A_2 与 A_3 两两垂直相交于坐标原点,建立坐标系如图3所示。对于供电电极 A_i ($i=1, 2, 3$),其坐标矢量用 $\mathbf{r}_{A_i}=(x_{A_i}, y_{A_i}, z_{A_i})$ 表示。式(7)可扩展^[42]为

$$\begin{aligned} [E_{11} \quad E_{21} \quad E_{31}] &= [\rho_{11} \quad \rho_{12} \quad \rho_{13}] [J_{11} \quad J_{21} \quad J_{31}] \\ E_{12} \quad E_{22} \quad E_{32} &= \rho_{21} \quad \rho_{22} \quad \rho_{23} \quad J_{12} \quad J_{22} \quad J_{32} \\ [E_{13} \quad E_{23} \quad E_{33}] &= [\rho_{31} \quad \rho_{32} \quad \rho_{33}] [J_{13} \quad J_{23} \quad J_{33}] \end{aligned} \quad (8)$$

由式(8)可得

式中, $K_1 = J_{1x}J_{2z} - J_{2y}J_{1z}$, $K_2 = J_{1y}J_{3z} - J_{3y}J_{1z}$, $K_3 = J_{2y}J_{3z} - J_{3y}J_{2z}$, $K_4 = J_{1x}J_{3z} - J_{3x}J_{1z}$, $K_5 = J_{1x}J_{2z} - J_{2y}J_{1z}$, $K_6 = J_{2x}J_{3z} - J_{3x}J_{2z}$, $K_7 = J_{1x}J_{2y} - J_{2x}J_{1y}$, $K_8 = J_{1x}J_{3y} - J_{3x}J_{1y}$, $K_9 = J_{2x}J_{3y} - J_{3x}J_{2y}$ 。

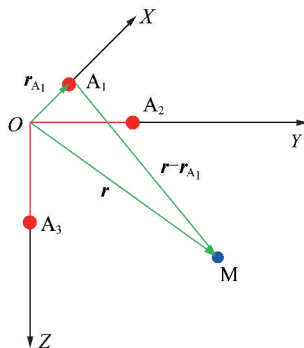


图3 张量电阻率测量原理

Fig. 3 Measurement principle of tensor resistivity

设供电电极 A_i 的矢径 $r_{A_i} = (x_{A_i}, y_{A_i}, z_{A_i})$, 则全空间任意场点 M (矢径为 $\mathbf{r} = (x, y, z)$)处的电流密度分量为

$$J_{ix} = \frac{I_i}{4\pi} \left(\frac{\mathbf{r} - \mathbf{r}_{A_i}}{|\mathbf{r} - \mathbf{r}_{A_i}|^3} \right) \cdot \mathbf{i} \quad (10)$$

$$J_{iy} = \frac{I_i}{4\pi} \left(\frac{\mathbf{r} - \mathbf{r}_{A_i}}{|\mathbf{r} - \mathbf{r}_{A_i}|^3} \right) \cdot \mathbf{j} \quad (11)$$

$$J_{iz} = \frac{I_i}{4\pi} \left(\frac{\mathbf{r} - \mathbf{r}_{A_i}}{|\mathbf{r} - \mathbf{r}_{A_i}|^3} \right) \cdot \mathbf{k} \quad (12)$$

式中, \mathbf{i}, \mathbf{j} 和 \mathbf{k} 分别为 X 轴、 Y 轴和 Z 轴的单位矢量; I_i 为供电电流强度。

式(9)中的电场强度可表示为电位函数的负梯度, 即

$$\mathbf{E}_i = -\operatorname{grad}(U_i) \quad (13)$$

式中, U_i 为任意点处的电位。

井下巷道空间为张量电阻率测量提供了十分便利的条件。如图4所示, 对于三极装置, 可以在巷道顶板、侧帮和底板上布置供电电极 A_1, A_2, A_3 和测量电极对 M_1, M_2, M_3 和 N , 供电和接收电极对两两垂直, 并分别相交于坐标原点和 N 点。当 A_1, A_2, A_3 分别供电时, 逐一测量 M_1, M_2, M_3 与 N 间的电位差, 即可得到电场强度分量, 从而根据式(9)计算获得张量电阻率的各分量。对于非均匀介质, 式(9)计算出的结果为视张量电阻率, 用 ρ_s^a 表示。

3 电各向异性的数值模拟与讨论

含煤地层具有成层分布的特征, 在顺层和垂直层面方向上的导电性具有明显差异, ZHDANOV 将这种导电性差异称为结构性各向异性^[43]。电阻率法(图5中 α 方向)正是利用这种宏观电各向异性达到定向

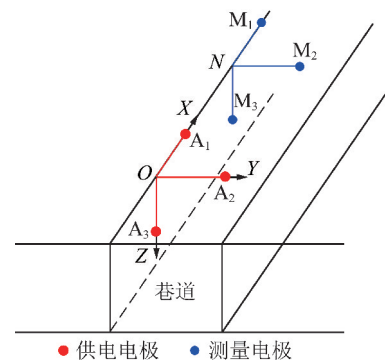


图4 巷道张量电阻率观测方式示意

Fig. 4 Sketch for resistivity tensor measurement

探测的目的。为了进行电各向异性特征研究, 文献[44]提出了一种层状介质的地面电阻率测量方式, 其中的供电 A 极在圆心处, 24 个 B 极点均匀布置在以 $AMNB$ 为半径的圆环上, 采用对称四极装置测量(图5)。当各层介质均匀各向同性时, 无论在地表还是巷道内测量(α 探测方向), 24 个测点的测量结果都相同。但是, 若煤层内存在断层、裂隙和破碎带等各向异性地质构造时, 传统的井下标量测量只能反映巷道顶、底板(α 方向)或顺煤层(β 方向)等特定方向的电性信息, 其他方向的电性变化则作为背景值受到压制。

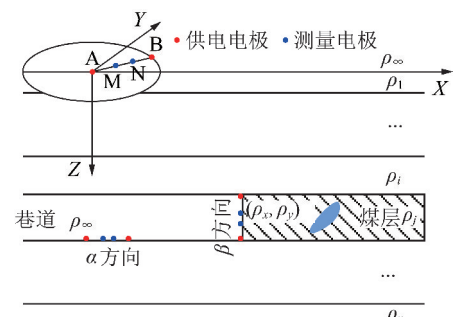


图5 层状介质电各向异性模型

Fig. 5 Anisotropic model for a layered medium

3.1 电各向异性特征

图6为两层介质的视电阻率方向特性, 该地电模型的第2层为各向异性介质, 地层倾角45°。由图6可以看出, 由于装置 B 极在 X 正、负轴上(1号和13号点)与各向异性地层的横向电阻率方向(n 方向)一致, 在 Y 正、负轴上(7号和19号点)与地层纵向电阻率方向(t 方向)一致, 因而在两坐标轴上得到的视电阻率分别达到了极大值和极小值, 该趋势与第2层两个方向的电阻率相对应。在 B 点所在的其他位置, 视电阻率值处于极大到极小(或极小到极大)的过渡阶段, 使视电阻率极化曲线呈椭圆型分布。由于视电阻率为第1, 2层介质电性的综合反映, 其大小与电阻率真值有一定差别, 但其变化规律揭示了第2层

介质的电各向异性特征。

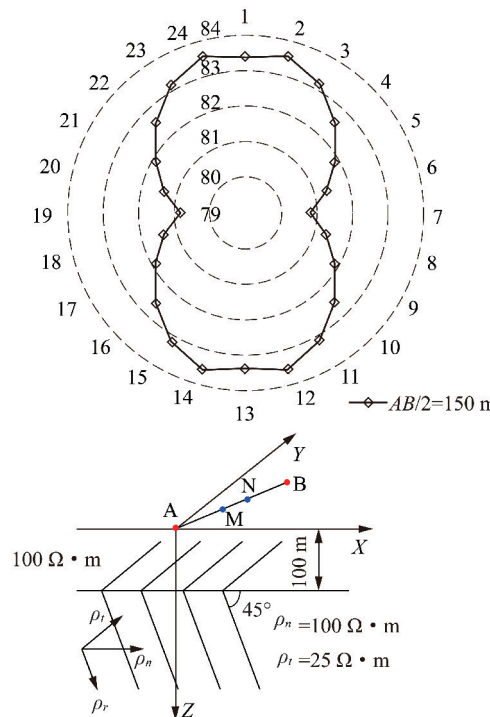


图6 两层介质的视电阻率($\Omega \cdot m$)方向特性

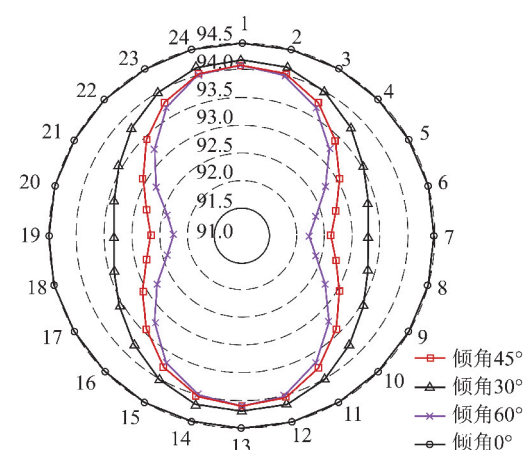
Fig. 6 Direction characteristics of apparent resistivity of two layered medium

裂隙带倾角和走向变化时的视电阻率方向特性如图7所示,模型中第2层为倾角和走向变化的裂隙带,厚度为20 m。分析图7可以得出:①倾角越小,介质各向异性的电阻率表现越弱,当倾角为0°时几乎无法分辨。倾角越大,椭圆长轴与短轴比例就越大;②介质各向异性的视电阻率幅值不受地层走向影响,但长轴绕中心旋转的角度依赖于地层走向;③各向异性地层的电阻率幅值受上覆和下伏地层电阻率影响,对于两图所示模型,尽管t方向电阻率为 $25 \Omega \cdot m$,是n方向的 $1/4$,但视电阻率均高于 $90 \Omega \cdot m$ 。

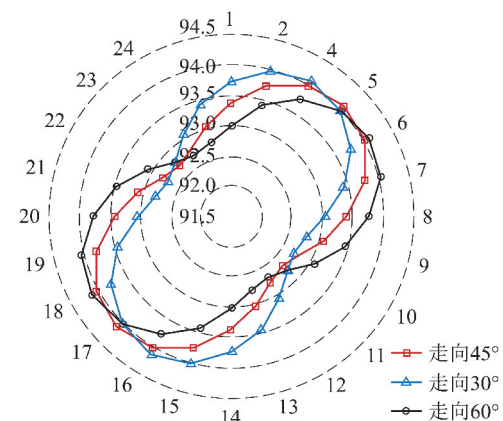
3.2 宏观电各向异性特征

层状介质具有结构性宏观电各向异性,巷道为层状介质内部的一个有限空腔,所充满的空气电阻率远高于围岩介质,更加强化了电各向异性特征。利用宏观电各向异性特征,可以对巷道顶、底板内的隐伏地质构造进行定位。

图8为一个底板有岩溶发育的全空间模型,供电点位于巷道底板,在顶、底板方向观测得到的视电阻率拟断面图如图9所示。图9底板下方岩溶的位置可以清楚辨识,表现为低阻异常的封闭区域,而在顶板方向的观测结果中该岩溶没有明显的地电异常反映。因此,矿井张量电阻率测量可以起到分辨目标体



(a) 倾角变化时



(b) 走向变化时

(a) 第2层倾角分别为 $0, 30^\circ, 45^\circ$ 和 60° ; (b) 第2层为各向异性介质,地层走向分别为 $30^\circ, 45^\circ$ 和 60°

图7 倾角和走向变化时3层介质的视电阻率($\Omega \cdot m$)方向特性

Fig. 7 Direction characteristics of apparent resistivity of three layered medium with different stratigraphic dips

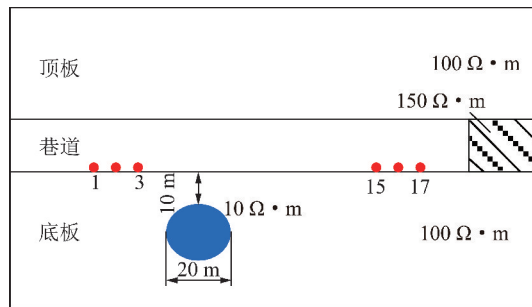


图8 巷道全空间介质模型

Fig. 8 Full-space model with roadway

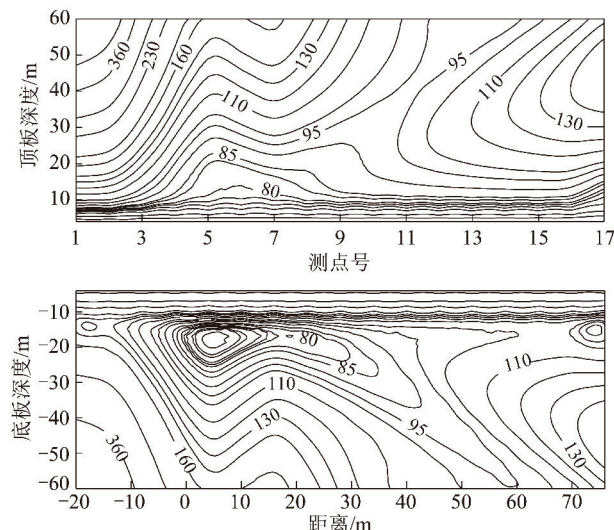


图9 视电阻率(Ω·m)拟断面

Fig. 9 Apparent resistivity section

空间方位的作用,同理亦可为局部各向异性目标体的精细探测提供数据支撑。

4 结论与展望

(1) 裂隙内水气富含程度对煤层横向和纵向电阻率产生明显影响,含水量越大,各向异性系数越高。

(2) 层状介质的宏观结构性各向异性和巷道空腔、地质构造引发的局部各向异性交织,增大了矿井电阻率精确测量的难度。改进观测方式,开发矿井电阻率张量测量是实现各向异性结构定位的有效方法之一。

煤矿动力灾害事故都有一个孕育、发展到发生的过程,通过理论方法创新,改变激励和接收方式,实现不同尺度、近远场耦合激励、全空间、多参数张量测量,掌握煤矿动力灾害致灾因素地电异常的时空演化特征,在不同空间和时间尺度上全面客观地研究采动岩体应力转移、结构演变和流体运动规律,才能在应力峰值到来之前、煤岩体未出现亚失稳状态的可逆阶段及时发现灾害孕育的先兆信息,为采取措施超前解除潜在生产安全威胁赢得时间。此外,基于5G技

术,在地面布置固定电磁发射基站、在井下设置可移动近场发射场源,通过井下电、磁传感器网络,实现全空间、全张量、多参数时频电磁实时动态监测的科学构想将成为可能。

参考文献(References):

- [1] YUE Jianhua, ZHANG Herui, YANG Haiyan, et al. Electrical prospecting methods for advance detection: Progress, problems, and prospects in Chinese coal mines[J]. IEEE Geoscience and Remote Sensing Magazine, 2019, 7(3): 94–106.
- [2] 岳建华,李志聃. 煤矿井下直流层测深方法与原理[J]. 煤炭学报, 1994, 19(4): 422–429.
- [3] YUE Jianhua, LI Zhidan. DC layer sounding in coal seams[J]. Journal of China Coal Society, 1994, 19(4): 422–429.
- [4] 岳建华,李志聃,刘世蕾. 巷道层测深理论曲线数值模拟及资料解释方法[J]. 煤田地质与勘探, 1997, 25(1): 54–58.
- [5] YUE Jianhua, LI Zhidan, LIU Shilei. Numerical simulation and data interpretation method of theoretical curves in coal seam sounding [J]. Coal Geology and Exploration, 1997, 25(1): 54–58.
- [6] 岳建华,李志聃,刘世蕾. 层状介质中巷道底板电测深边界元法正演[J]. 煤炭学报, 1998, 23(4): 13–17.
- [7] YUE Jianhua, LI Zhidan, LIU Shilei. Modeling of floor sounding in roadway in a layered medium by boundary element method[J]. Journal of China Coal Society, 1998, 23(4): 13–17.
- [8] 岳建华,李志聃. 矿井直流电法勘探中的巷道影响[J]. 煤炭学报, 1999, 24(1): 7–10.
- [9] YUE Jianhua, LI Zhidan. Roadway influence on electrical prospecting in underground mine[J]. Journal of China Coal Society, 1999, 24(1): 7–10.
- [10] 岳建华,刘树才. 矿井直流电法勘探[M]. 徐州:中国矿业大学出版社, 2000.
- [11] 程久龙,王玉和,于师建,等. 巷道掘进中电阻率法超前探测原理与应用[J]. 煤田地质与勘探, 2000, 28(4): 60–62.
- [12] CHENG Jiulong, WANG Yuhe, YU Shijian, et al. The principle and application of advance surveying in roadway excavation by resistivity method[J]. Coal Geology and Exploration, 2000, 28(4): 60–62.
- [13] 刘树才,刘志新,姜志海,等. 矿井直流电法三维正演计算若干问题[J]. 物探与化探, 2004, 28(2): 170–172, 176.
- [14] LIU Shucui, LIU Zhixin, JIANG Zhihai, et al. Some problems in 3D forward simulation of mine direct current method[J]. Geophysical and Geochemical Exploration, 2004, 28(2): 170–172, 176.
- [15] 黄俊革,鲍光淑,阮百尧. 坑道直流电阻率测深异常研究[J]. 地球物理学报, 2005, 48(1): 222–228.
- [16] HUANG Junge, BAO Guangshu, RUAN Baiyao. A study on anomalous bodies of DC resistivity sounding in tunnel[J]. Chinese Journal of Geophysics, 2005, 48(1): 222–228.
- [17] 韩德品,李丹,程久龙,等. 超前探测灾害性含导水地质构造的直流电法[J]. 煤炭学报, 2010, 35(4): 635–639.
- [18] HAN Depin, LI Dan, CHENG Jiulong, et al. DC method of advanced detecting disastrous water-conducting or water-bearing geological structures along same layer[J]. Journal of China Coal Society, 2010, 35(4): 635–639.

- [11] 柳建新, 邓小康, 郭荣文, 等. 坑道直流聚焦超前探测电阻率法有限元数值模拟 [J]. 中国有色金属学报, 2012, 22(3): 970–975.
LIU Jianxin, DENG Xiaokang, GUO Rongwen, et al. Numerical simulation of advanced detection with DC focus resistivity in tunnel by finite element method [J]. The Chinese Journal of Nonferrous Metals, 2012, 22(3): 970–975.
- [12] 鲁晶津, 吴小平. 巷道直流电阻率法超前探测三维数值模拟 [J]. 煤田地质与勘探, 2013, 41(6): 83–86.
LU Jingjin, WU Xiaoping. 3D numerical modeling of tunnel DC resistivity for inadvance detection [J]. Coal Geology and Exploration, 2013, 41(6): 83–86.
- [13] 李术才, 聂利超, 刘斌, 等. 多同性源阵列电阻率法隧道超前探测方法与物理模拟试验研究 [J]. 地球物理学报, 2015, 58(4): 1434–1446.
LI Shucai, NIE Lichao, LIU Bin, et al. Advanced detection and physical model test based on multi-electrode sources array resistivity method in tunnel [J]. Chinese Journal of Geophysics, 2015, 58(4): 1434–1446.
- [14] 袁亮, 张平松. 煤炭精准开采地质保障技术的发展现状及展望 [J]. 煤炭学报, 2019, 44(8): 2277–2284.
YUAN Liang, ZHANG Pingsong. Development status and prospect of geological guarantee technology for precise coal mining [J]. Journal of China Coal Society, 2019, 44(8): 2277–2284.
- [15] 程久龙, 李飞, 彭苏萍, 等. 矿井巷道地球物理方法超前探测研究进展与展望 [J]. 煤炭学报, 2014, 39(8): 1742–1750.
CHENG Jiulong, LI Fei, PENG Suping, et al. Research progress and development direction on advanced detection in mine roadway working face using geophysical methods [J]. Journal of China Coal Society, 2014, 39(8): 1742–1750.
- [16] 李术才, 李凯, 翟明华, 等. 矿井地面-井下电性源瞬变电磁探测响应规律分析 [J]. 煤炭学报, 2016, 41(8): 2024–2032.
LI Shucai, LI Kai, ZHAI Minghua, et al. Analysis of grounded Transient Electromagnetic with surface-tunnel configuration in mining [J]. Journal of China Coal Society, 2016, 41(8): 2024–2032.
- [17] 于景春, 苏本玉, 薛国强, 等. 煤层顶板致灾水体井上下双磁源瞬变电磁响应及应用 [J]. 煤炭学报, 2019, 44(8): 2356–2360.
YU Jingcun, SU Benyu, XUE Guoqiang, et al. Transient electromagnetic response of double magnetic source in coal seam roof disaster caused by water and its application [J]. Journal of China Coal Society, 2019, 44(8): 2356–2360.
- [18] 程久龙, 黄少华, 温来福, 等. 矿井全空间三维主轴各向异性介质瞬变电磁场响应特征研究 [J]. 煤炭学报, 2019, 44(1): 278–286.
CHENG Jiulong, HUANG Shaohua, WEN Laifu, et al. Response characteristics of three-dimensional axial anisotropic media for transient electromagnetic method in underground whole-space [J]. Journal of China Coal Society, 2019, 44(1): 278–286.
- [19] 程久龙, 赵家宏, 董毅, 等. 基于 LBA-BP 的矿井瞬变电磁法岩层富水性的定量预测 [J]. 煤炭学报, 2020, 45(1): 330–337.
CHENG Jiulong, ZHAO Jiahong, DONG Yi, et al. Quantitative prediction of water abundance in rock mass by transient electro-magnetic method with LBA-BP neural network [J]. Journal of China Coal Society, 2020, 45(1): 330–337.
- [20] ZHDANOV M S. Foundations of geophysical electromagnetic theory and methods [M]. New York, Tokyo: Elsevier, Amsterdam, 2018.
- [21] BRACE W F, ORANGE A F. Electrical resistivity changes in saturation rocks during fracture and frictional sliding [J]. J. Geophys. Res., 1968, 73: 1433–1445.
- [22] POWER W L, TULLIS T E, et al. Roughness of natural faults surface [J]. Geophysics Research Letter, 1987, 14: 29–32.
- [23] KELLER G V, FRISCHKNECHT F C. Electrical methods in geophysical prospecting [M]. Orford: Pergamon Press, 1966.
- [24] STESKY R M. Electrical conductivity of brine saturated fractured rock [J]. Geophysics, 1986, 51(8): 1585–1593.
- [25] 吕绍林, 何继善. 瓦斯突出煤体的导电性质研究 [J]. 中南工业大学学报, 1998, 29(6): 511–514.
LÜ Shaolin, HE Jishan. Electrical property measurements for the outburst coal mass [J]. Journal of Central South University of Technology (Natural Science), 1998, 29(6): 511–514.
- [26] 陈鹏. 煤与瓦斯突出区域危险性的直流电法响应及应用研究 [D]. 徐州: 中国矿业大学, 2013.
CHEN Peng. Direct current electric method response of regional coal and gas outburst danger and its application [D]. Xuzhou: China University of Mining and Technology, 2013.
- [27] 王蕃树. 大震前地电阻率各向异性变化的研究 [J]. 华北地震科学, 1984, 2(2): 48–53.
WANG Fanshu. A study on the change of the anisotropy of earth resistivity before large earthquake [J]. North China Earthquake Science, 1984, 2(2): 48–53.
- [28] ALEKSEEV A S, TSIBULCHIK G M, KOVALEVSKY V V, et al. Elements of Active Geophysical Monitoring Theory [A]. JUNZO Kasahara, VALERI Kornev, MICHAEL S Zhdanov. Active Geophysical Monitoring (Handbook of Geophysical Exploration Seismic Exploration) [C]. Elsevier Science, 2010.
- [29] SU B Y, YUE J H. Research of the electrical anisotropic characteristics of water-conducting fractured zones in coal seams [J]. Applied Geophysics, 2017, 14(2): 216–224.
- [30] 袁亮. 煤矿典型动力灾害风险判识及监控预警技术研究进展 [J]. 煤炭学报, 2020, 45(5): 1557–1566.
YUAN Liang. Research progress on risk identification, assessment, monitoring and early warning technologies of typical dynamic hazards in coal mines [J]. Journal of China Coal Society, 2020, 45(5): 1557–1566.
- [31] 舒勇龙, 朱南南, 陈洁, 等. 煤与瓦斯突出危险精准辨识理论方法与技术探索 [J]. 煤炭学报, 2020, 45(5): 1614–1625.
SHU Longyong, ZHU Nannan, CHEN Jie, et al. Theoretical method and technology of precision identification for coal and gas outburst hazard [J]. Journal of China Coal Society, 2020, 45(5): 1614–1625.
- [32] BIBBY H M. The apparent resistivity tensor [J]. Geophysics, 1977, 42: 1258–1261.
- [33] BIBBY H M, HOHMANN G W. Three-dimensional interpretation of multiple-source bipole-dipole resistivity data using the apparent resistivity tensor [J]. Geophysical Prospecting, 1993, 41: 697–723.
- [34] BIBBY H M. Analysis of multiple-source bipole-quadrupole resistiv-

- ity surveys using the apparent resistivity tensor [J]. Geophysics, 1986, 51:972–983.
- [35] АКУЛЕНКО С А, БЕРЕЗИНА С А, и др. Электроразведка методом сопротивлений [M]. МГУ, 1994.
- [36] MODIN I N, PERVAGO E V, SHEVNIN V A, et al. Vector measurements in resistivity prospecting [A]. EAEG Meeting [C]. 1994.
- [37] FIORE B D, MAURIELLO P, MONNA D, et al. Examples of application of tensorial resistivity probability tomography to architectonic and archaeological targets [J]. Annali Di Geofisica, 2002, 45 (2): 417–430.
- [38] MAURIELLO P. Resistivity tensor probability tomography [J]. Progress in Electromagnetics RESEARCH B, 2008 (8): 129–146.
- [39] ALEXEY Bobachev, BOLSHAKOV D K, MODIN I N. The study of the anisotropy in the resistivity method [M]. Moscow: Moscow State University, 2012.
- [40] SHEN J S, LIU Z X, WANG S H, et al. Analysis of the mechanism of the effects of secondary porosities on the cementation factor and saturation index in reservoir formation with vuggs and fractures [J]. Well Logging Technology, 2010, 34 (1): 9–15.
- [41] 克拉耶夫. 地电原理 [M]. 张可迁, 陈培光, 张志诚, 等译. 北京: 地质出版社, 1954.
- [42] ONSAGER L. Reciprocal relations in irreversible processes. I [J]. Physical Review, 1931, 37: 405–426.
- [43] ZHDANOV M S. Foundations of geophysical electromagnetic theory and methods [M]. Elsevier, Amsterdam-New York, Tokyo, 2018.
- [44] YIN C C, WEIDELT P. Geoelectrical fields in a layered earth with arbitrary anisotropy [J]. Geophysics, 1999, 64 (2): 426–434.